Instabilities near Ultrastrong Coupling in a Microwave Optomechanical Cavity

Soumya Ranjan Das, Sourav Majumder, Sudhir Kumar Sahu, Ujjawal Singhal, Tanmoy Bera, and Vibhor Singh*
Department of Physics, Indian Institute of Science, Bangalore-560012, India

(Received 2 February 2023; revised 3 July 2023; accepted 19 July 2023; published 7 August 2023)

With artificially engineered systems, it is now possible to realize the coherent interaction rate, which can become comparable to the mode frequencies, a regime known as ultrastrong coupling (USC). We experimentally realize a cavity-electromechanical device using a superconducting waveguide cavity and a mechanical resonator. In the presence of a strong pump, the mechanical-polaritons splitting can nearly reach 81% of the mechanical frequency, overwhelming all the dissipation rates. Approaching the USC limit, the steady-state response becomes unstable. We systematically measure the boundary of the unstable response while varying the pump parameters. The unstable dynamics display rich phases, such as self-induced oscillations, period-doubling bifurcation, and period-tripling oscillations, ultimately leading to the chaotic behavior. The experimental results and their theoretical modeling suggest the importance of residual nonlinear interaction terms in the weak-dissipative regime.

DOI: 10.1103/PhysRevLett.131.067001

Introduction.—Radiation-pressure interaction is fundamental to the cavity-optomechanical systems consisting of a mechanical mode coupled to an electromagnetic mode (EM) [1]. With technological advancements, cavity optomechanical devices have been successful in controlling the low-frequency mechanical mode down to their quantum regime [2]. Several demonstrations pertaining to the quantum state preparation [3–6] and entanglement [7–10], signal transduction [11–13], and topological physics using the mechanical modes have been shown [14,15].

The coherent coupling rate, characterizing the interaction between the EM mode (ω_c) and the mechanical mode (ω_m), is a key figure of merit in such devices [1,2]. The energy dissipation rates of the two modes (κ, γ_m) capture the incoherent coupling with their thermal baths. Based on the relative strengths of these rates, several interesting scenarios are feasible. When the coherent coupling rate (g) exceeds the dissipative coupling rates of the two modes $(g \gg \kappa, \gamma_m)$, the two modes hybridize, resulting in new eigenstates [16,17]. Further, when the coherent coupling rate becomes a significant fraction of the mode frequencies, the composite system enters the "ultrastrong coupling" (USC) limit [18]. In this limit, the two modes hybridize in a nontrivial way leading to an entangled ground state in the quantum regime [19,20]. The USC limit has been experimentally demonstrated in several systems where two modes interact nearly resonantly [21,22].

In cavity optomechanical systems, however, the EM mode and mechanical mode interact dispersively $(\omega_c \gg \omega_m)$. The nonlinear radiation-pressure interaction can be described by $H_i/\hbar = -g_0 a^\dagger a(b + b^\dagger)$, where g_0 is the single-photon coupling strength and $a(b)$'s are the ladder operators for the cavity(mechanical) mode. In the presence of a strong coherent pump, the interaction Hamiltonian can be linearized to $H_i/\hbar \simeq -g(a + a^\dagger) \times (b + b^\dagger)$, where $g = g_0\sqrt{n_d}$ is the parametric coupling rate and n_d is the number of the pump photons in the cavity. With the ability to control the parametric coupling rate, several regimes, such as quantum coherent coupling, and steady-state quantum entanglement between the two modes

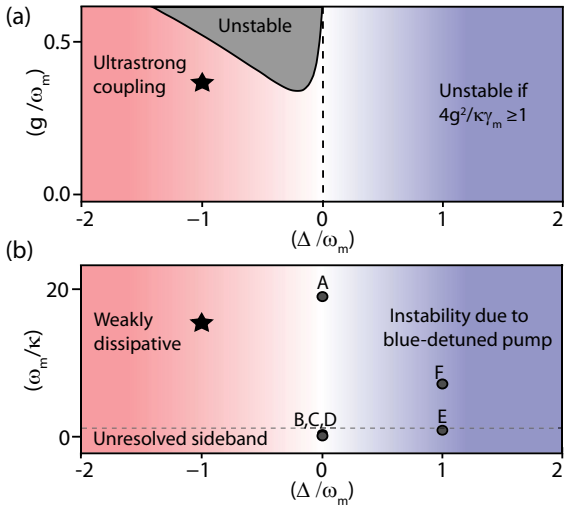

FIG. 1. (a) The schematic of the parameter space of a cavity-electromechanical system in the steady state marking the USC regime and the region of unstable response. This study has been marked by star. (b) Comparison of the sideband-resolution parameter of this study and the earlier studies on instabilities. The data points A to F are from Refs. [24–29], respectively. The symbols g, ω_m, κ, and Δ represent the optomechanical coupling strength, the mechanical frequency, cavity dissipation rate, and the pump detuning from the cavity resonant frequency, respectively.

can be reached [10,17,23]. Ultimately, owing to the nonlinear nature of the radiation-pressure interaction, the response becomes unstable, as shown schematically in Fig. 1.

Indeed, various phenomena in the unstable region such as limit cycle, period doubling bifurcations, and chaos have been extensively studied [30–34]. Experimentally, these effects have been primarily explored in the strong dissipative regime ($\omega_m \lesssim \kappa$) or with the blue-detuned pump [24–29,35] (see Fig. 1). The instabilities near the ultrastrong coupling limit, however, allow one to explore the nonlinear dynamics of the cavity optomechanical system in the *weakly dissipative* limit ($\gamma_m, \kappa \ll 2g \lesssim \omega_m$). The nonlinear dynamics with weak dissipation is unique and is predicted to show transient chaos, a quasiperiodic route to chaos, and lower threshold powers for the onset of chaos [36,37].

Here, we use a cavity-electromechanical device in the microwave domain to probe the route to chaos when it is operated into the USC limit. We first demonstrate the USC by performing the spectroscopic and time-domain measurements. We probe the stability of the device when the pump detuning near the red sideband and injected power are varied. The unstable region shows very rich phases in the parameter space, such as the self-induced oscillation, period-doubling bifurcations, period-tripling oscillations, and chaotic behavior [32,36,37]. We find that the measured threshold powers for the onset of instabilities are lower than the ones predicted from a nonlinear model considering the optomechanical interaction and a Kerr-term in the cavity.

Experimental details.—We use the three-dimensional cavity-based platform to realize the cavity-electromechanical device [38–40]. The waveguide cavity-based electromechanical device offers a higher dynamic range for the pumped photons, which is highly desirable to reach the USC limit [40,41]. As shown in Figs. 2(a) and 2(b), the device consists of a rectangular waveguide cavity, and a drumhead-shaped mechanical resonator in the form of a parallel plate capacitor patterned on a sapphire chip. The patterned sapphire chip fabricated with aluminum is placed at the center of the cavity. The electrical pads to the drumhead are then directly wire-bonded to the cavity walls to integrate with the cavity mode [40].

The sample-mounted cavity is cooled down to 20 mK in a dilution fridge. Figure 2(c) shows the measurement of the cavity transmission at the base temperature. The bare cavity is designed to have the fundamental resonant mode frequency of 7.5 GHz. However, the electromechanical capacitor perturbs the mode shape significantly, and lowers the mode frequency to $\omega_c/2\pi \approx 4.86$ GHz. The reduction in the resonant frequency of the cavity results from the electromechanical capacitance and the inductance of the connecting electrodes introduced after the addition of a patterned sapphire chip. We measure the input, output, and the internal dissipation rates of $\kappa_{e1}/2\pi \approx 90$ kHz, $\kappa_{e2}/2\pi \approx 190$ kHz, and $\kappa_i/2\pi \approx 100$ kHz, respectively. At low temperatures, we estimated that the gap between the electromechanical

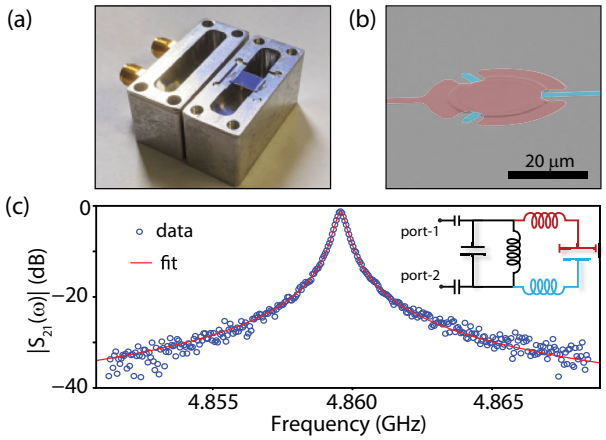

FIG. 2. (a) Image of the waveguide cavity along with a patterned substrate. The cavity has dimensions of $26 \times 26 \times 6$ mm^3. (b) False color image of the mechanical resonator forming a parallel plate capacitor with another plate on the substrate. The separation between the capacitor plates at room temperature is approximately 200 nm. (c) Measurement of the voltage transmission coefficient $|S_{21}|$ of the device at the base temperature. The inset shows the equivalent circuit diagram of the cavity electromechanical device.

capacitor plates reduces to approximately 32 nm due to thermal contraction [42,43], which helps in achieving a single photon coupling rate $g_0/2\pi$ of 165 Hz.

Ultrastrong coupling regime.—We measure the transmission coefficient $|S_{21}(\omega)|$ through the cavity using a weak probe tone while injecting a pump detuned near the red sideband $\omega_c - \omega_m$. At relatively lower pump powers, the optomechanically induced absorption setup allows us to determine the mechanical frequency $\omega_m/2\pi \approx 6.32$ MHz [44]. At relatively higher pump powers, the response turns into two well-separated peaks confirming the new eigenmodes of the system as shown in Fig. 3(a). The peak separation being $0.81\omega_m$ marks the ultrastrong coupling between the mechanical resonator and the cavity. The transmission measurement shows the presence of an additional weakly coupled mechanical mode, indicated by the red arrow. Two more features arising from the interference of the down-scattered pump signal and the probe signal can be seen. Figure 3(b) shows the measurement of $|S_{21}|$ as the frequency of the pump is varied while maintaining a constant power at the signal generator.

The presence of a strong intracavity pump field leads to a static shift of the equilibrium position of the mechanical resonator, given by $x_s = (2g_0 n_d/\omega_m)x_{zp}$, where x_{zp} is the zero-point motion of the mechanical resonator. The shift in the equilibrium position of the mechanical resonator leads to a Kerr shift of the cavity frequency by $-2g_0^2 n_d/\omega_m$. The total shift in the cavity frequency comes from the static nature of the radiation-pressure force and nonlinear kinetic inductance of the superconducting aluminum film. We emphasize here that at high pump powers, the Kerr shift of

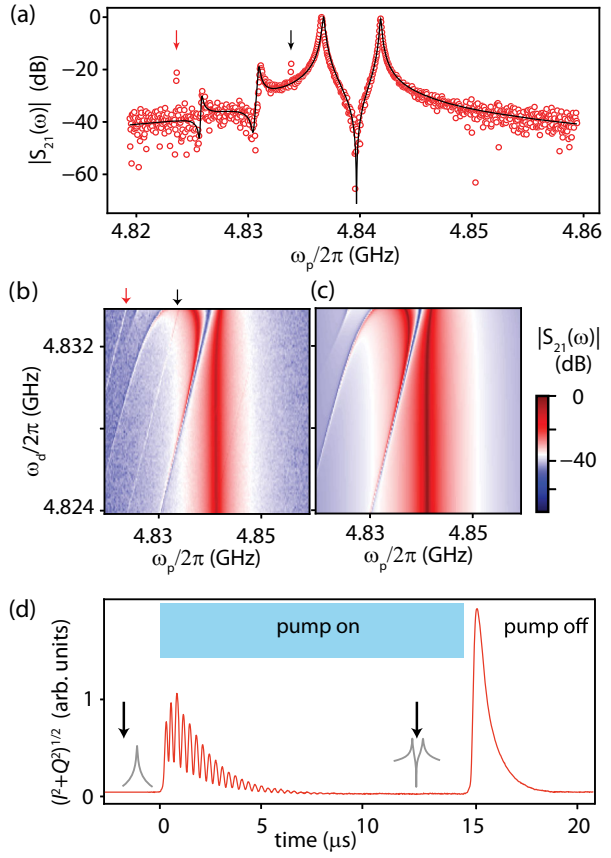

FIG. 3. (a) The normalized magnitude of the cavity transmission $|S_{21}(\omega)|$ (red circles) while applying a strong pump near the red sideband. The black line shows the calculated $|S_{21}(\omega)|$ while including the static Kerr shift of the cavity. (b) The colorplot of measured $|S_{21}(\omega)|$ as the pump frequency ω_d is varied at a fixed pump power of −31 dBm at the cavity. The black arrow shows the position of the pump signal, while the red arrow indicates another weakly coupled mechanical mode. A weak probe signal −88 dBm at the cavity is used to generate the colorplot. (c) Colorplot of $|S_{21}(\omega)|$ obtained from the calculations. (d) Measurement of the amplitude of the transmitted probe signal in the time domain while modulating the interaction strength. The pump frequency is set near the lower mechanical sideband. The position of the probe signal is schematically represented by the black arrows relative to the steady-state cavity transmission curves (shown in gray).

the cavity becomes significant, and it must be considered to capture the cavity transmission faithfully. In this case, we found a cavity shift of ∼1.76 MHz at the maximum pump power used in the experiment. It corresponds to an optomechanical Kerr coefficient of 8.6 mHz/photon and a kinetic inductance Kerr coefficient of approximately 5 mHz/photon at the maximum pump power (see the Supplemental Material [45]).

To theoretically model the cavity transmission, we expand the interaction Hamiltonian H_i around the mean field of the pump and obtain the quantum-Langevin equations of motion. Without using the rotating-wave approximation and by retaining the static Kerr shift of the cavity frequency, the steady-state response can be obtained from the inverse of the mode-coupling matrix (see the Supplemental Material [45]). The solid line in Fig. 3(a) and colorplot in Fig. 3(c) show the calculated transmission coefficient using the experimentally determined device parameters. While in general, additional weakly coupled mechanical modes can also be included in the calculations, we neglect them here for simplicity.

The onset of the strong coupling allows for a coherent swap of the excitations between the cavity and the mechanical mode. It thus enables the high-speed optomechanical swap gates in the ultrastrong coupling limit. To explore the maximum speed of the optomechanical swap, we perform time-domain measurements in this limit. We modulate the interaction strength $g(t)$, which is controlled by the amplitude of the pump tone. The transmission through the cavity is monitored by applying a weak continuous probe signal near ω_c. To demodulate the probe signal, we first mix it down using an external mixer and then sending it to a high-speed lock-in amplifier to further demodulate the quadratures with a short integration time (100 ns) (see the Supplemental Material [45]).

Figure 3(d) shows the measurement of the magnitude of the demodulated signals $[I(t), Q(t)]$ as the interaction strength $g(t)$ is modulated. For this measurement, the interaction strength is modulated to 1.55 MHz. The probe frequency is detuned from the cavity resonant frequency by $(\omega_p - \omega_c)/2\pi = 372$ kHz. Therefore, the transmission is small even when the pump tone is off ($t < 0$). In the steady-state when the pump is turned on ($t \approx 10$ μs), the transmission is low again due to the formation of mechanical-polariton modes. Because of the strong static Kerr shift of the cavity, the probe tone appears near the center of the split peaks, resulting in low transmission.

When interaction is just switched on, the transient response shows the oscillations arising from the coherent energy exchange between the mechanical and the cavity modes. The oscillation frequency of 3.1 MHz corresponds to the characteristic swap time of 160 ns. The amplitude of the oscillations decays at a rate of $\simeq\kappa/4$ set by joint dissipation of the two polaritons. When the pump is turned off, the energy stored in the two polariton modes reemerges near the probe frequency, and the amplitude decays at $\kappa/2$. It is important to remark that as we operate close to the USC limit, the modulated pump signal spectrally overlaps with the probe signal and adds a small offset in the measurement. Additional datasets are provided in the Supplemental Material [45].

Parametic instabilities near ultrastrong coupling.— After establishing the USC in the present experiment, we now discuss the parametric instabilities arising at the high pump powers. At the core of it, the instabilities stem from the nonlinear interaction between the microwave field and the mechanical motion. To experimentally investigate

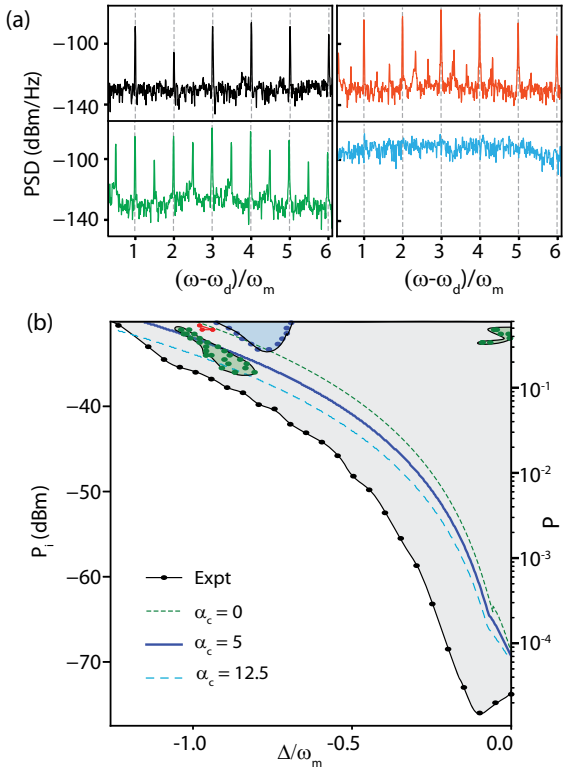

FIG. 4. (a) Measurement of the single sideband microwave power spectral density (PSD) for different injected pump powers P_i. Different panels show the self-induced oscillations (black), first period-doubling bifurcations (green), period-tripling oscillations (red), and the chaotic behavior (blue). (b) The gray region represents the boundary of self-induced oscillations. The black circles are the experimentally measured points. At higher injected pump powers, the region of period-doubling bifurcations is represented by the green region. The period-tripled oscillations are shown by the red-colored region. The region of chaotic behavior is shown by the cyan-colored region. Experimentally measured points are shown by the circles of different colors. The solid blue line and the dashed lines show the unstable boundary obtained from the theoretical calculation.

the phase space of the parametric instabilities and their nature, we measure the microwave power spectral density (PSD) using a spectrum analyzer while varying the pump power P_i and pump detuning $\Delta = (\omega_d - \omega_c)$. As P_i is increased, the self-induced oscillations appear as multiple peaks separated by ω_m in the microwave PSD. Figure 4(a) shows the PSD of different kinds of responses. The top-left panel corresponds to the instability due to the self-induced oscillations where the peaks are separated by ω_m. The bottom-left panel corresponds to the first period-doubling bifurcations (PDB), where the peaks are separated by $\omega_m/2$. The top-right panel shows the period-tripled oscillations where the peaks are separated by $\omega_m/3$. The bottom-right panel shows the response where the power is uniformly distributed over a broad range of frequencies. It corresponds to the chaotic vibration of the mechanical oscillator undergoing aperiodic oscillations leading to a continuous power spectrum in the output microwave field. These different phases of unstable response are summarized in Fig. 4(b). The gray-color region represents the parametrically unstable response. The boundary of the gray region marks the threshold power for the self-induced oscillations. With a decrease in Δ, the circulating power in the cavity decreases, and the threshold power for the onset of the instability increases. The regions of first PDB, period-tripled oscillations, and chaos are color coded within the unstable region. A discussion on the measurement methodology is included in the Supplemental Material [45].

To understand these results, we use the classical nonlinear dynamics approach. We start with the full cavity optomechanical Hamiltonian, i.e., $H_i/\hbar = -g_0\hat{a}^\dagger\hat{a}(\hat{b} + \hat{b}^\dagger)$. In addition, motivated by the observation of period-tripling oscillations and the relevance of the kinetic inductance at the high pump powers, we include a weak nonlinear term in the cavity Hamiltonian, given by $-(\alpha_c/2)(\hat{a}^\dagger\hat{a})^2$. Using the semiclassical approximation, we obtain the classical equations of motion (EOM) for the cavity and the mechanical quadratures. From EOMs, we find the fixed points and perform a linear stability test, which is similar to the Routh-Hurwitz criteria, i.e., the solutions are stable if and only if all the eigenvalues of the evolution matrix of small perturbations around the fixed points have a negative real part [48]. Calculation details are provided in the Supplemental Material [45].

Results of these calculations in different limits are shown in Fig. 4(b). We also include a dimensionless power $P = 8g_0^2 n_0/\omega_m^4$ on the right y axis, where n_0 is defined as the number of photons when the pump is set at the cavity frequency [32,37]. Clearly, the threshold power estimated from the calculations is larger than the one measured in the experiment. For comparison, the instability boundary obtained while considering the optomechanical Kerr nonlinearity alone ($\alpha_c = 0$), and two nonzero values of $\alpha_c/2\pi = 5$, 12.5 mHz/photon are also included. We note that even a significantly higher value of α_c does not fully explain the experimental findings suggesting a different origin. Thus, the nonlinearities arising from the optomechanical interaction and the kinetic inductance do not completely capture the threshold for the unstable region when a linear stability test is applied.

In addition, the numerical calculations do not show the period-doubling bifurcations or chaotic behavior for the pump parameters used in the experiment. In numerical calculations, these effects appear at higher powers than the ones observed in the experiment. It thus provides the first experimental evidence that the route to chaos in the USC limit or equivalently in the weakly dissipative limit is different from the previously studied cases. It suggests that the role of thermal fluctuations, and residual weak nonlinear coupling terms might be relevant in determining the boundary of the unstable region [49,50]. In particular, during the transitions from self-oscillation to period-doubling

oscillation and subsequently to chaotic regions, the mechanical mode remains in a high amplitude state. In this case, the role of mechanical Duffing nonlinearity, and resonantly induced negative dissipation might become important [51].

Outlook and conclusion.—In conclusion, we have demonstrated the ultrastrong coupling using a superconducting waveguide cavity and a mechanical resonator, where the splitting of the mechanical polaritons becomes nearly 81% of the mechanical frequency. In the time domain, we measure optomechanical swap time of 160 ns, which is nearly 16 times shorter than the shortest dissipation time in the device. With suitable modification to the thermalization of the microwave signals, the cavity can be operated in the quantum limit. It would enable a wide variety of experiments such as the entangled ground state properties of the cavity and the mechanical resonator [22], and high speed optomechanical gates [43]. Using the pump in a pulse mode, the parametric coupling can be pushed beyond the USC regime [20,52]. In addition, the microwave frequency comb generated using the optomechanical nonlinearity can be a valuable resource for sensing applications [36]. The experiment here, for the first time, explores the unstable response in the steady state in the weakly dissipative limit [37]. Clearly, the theoretical model based on optomechanical and kinetic inductance nonlinearity does not account for the lower threshold powers observed in the experiment. It thus opens up the possibility of further exploring the role of quantum fluctuations [32], and other weak residual couplings in the interaction Hamiltonian [49].

The authors thank G. S. Agarwal, Manas Kulkarni, and Tamoghana Ray for their valuable discussions. This material is based upon work supported by the Air Force Office of Scientific Research under Award No. FA2386-20-1-4003. V. S. acknowledges the support received under the Core Research Grant by the Department of Science and Technology (India). The authors acknowledge device fabrication facilities at CeNSE, IISc Bangalore, and central facilities at the Department of Physics funded by DST (Govt. of India).

*v.singh@iisc.ac.in

[1] M. Aspelmeyer, T. J. Kippenberg, and F. Marquardt, Cavity optomechanics, Rev. Mod. Phys. **86**, 1391 (2014).
[2] S. Barzanjeh, A. Xuereb, S. Gröblacher, M. Paternostro, C. A. Regal, and E. M. Weig, Optomechanics for quantum technologies, Nat. Phys. **18**, 15 (2022).
[3] J. D. Teufel, T. Donner, D. Li, J. W. Harlow, M. S. Allman, K. Cicak, A. J. Sirois, J. D. Whittaker, K. W. Lehnert, and R. W. Simmonds, Sideband cooling of micromechanical motion to the quantum ground state, Nature (London) **475**, 359 (2011).
[4] J. Chan, T. P. M. Alegre, A. H. Safavi-Naeini, J. T. Hill, A. Krause, S. Gröblacher, M. Aspelmeyer, and O. Painter, Laser cooling of a nanomechanical oscillator into its quantum ground state, Nature (London) **478**, 89 (2011).
[5] E. A. Wollack, A. Y. Cleland, R. G. Gruenke, Z. Wang, P. Arrangoiz-Arriola, and A. H. Safavi-Naeini, Quantum state preparation and tomography of entangled mechanical resonators, Nature (London) **604**, 463 (2022).
[6] M. Bild, M. Fadel, Y. Yang, U. von Lüpke, P. Martin, A. Bruno, and Y. Chu, Schrödinger cat states of a 16-microgram mechanical oscillator, Science **380**, 274 (2023).
[7] T. A. Palomaki, J. W. Harlow, J. D. Teufel, R. W. Simmonds, and K. W. Lehnert, Coherent state transfer between itinerant microwave fields and a mechanical oscillator, Nature (London) **495**, 210 (2013).
[8] R. Riedinger, A. Wallucks, I. Marinković, C. Löschnauer, M. Aspelmeyer, S. Hong, and S. Gröblacher, Remote quantum entanglement between two micromechanical oscillators, Nature (London) **556**, 473 (2018).
[9] C. F. Ockeloen-Korppi, E. Damskägg, J.-M. Pirkkalainen, M. Asjad, A. A. Clerk, F. Massel, M. J. Woolley, and M. A. Sillanpää, Stabilized entanglement of massive mechanical oscillators, Nature (London) **556**, 478 (2018).
[10] S. Kotler, G. A. Peterson, E. Shojaee, F. Lecocq, K. Cicak, A. Kwiatkowski, S. Geller, S. Glancy, E. Knill, R. W. Simmonds, J. Aumentado, and J. D. Teufel, Direct observation of deterministic macroscopic entanglement, Science **372**, 622 (2021).
[11] R. W. Andrews, R. W. Peterson, T. P. Purdy, K. Cicak, R. W. Simmonds, C. A. Regal, and K. W. Lehnert, Bidirectional and efficient conversion between microwave and optical light, Nat. Phys. **10**, 321 (2014).
[12] M. Forsch, R. Stockill, A. Wallucks, I. Marinković, C. Gärtner, R. A. Norte, F. van Otten, A. Fiore, K. Srinivasan, and S. Gröblacher, Microwave-to-optics conversion using a mechanical oscillator in its quantum ground state, Nat. Phys. **16**, 69 (2020).
[13] M. Mirhosseini, A. Sipahigil, M. Kalaee, and O. Painter, Superconducting qubit to optical photon transduction, Nature (London) **588**, 599 (2020).
[14] J. Cha, K. W. Kim, and C. Daraio, Experimental realization of on-chip topological nanoelectromechanical metamaterials, Nature (London) **564**, 229 (2018).
[15] A. Youssefi, S. Kono, A. Bancora, M. Chegnizadeh, J. Pan, T. Vovk, and T. J. Kippenberg, Topological lattices realized in superconducting circuit optomechanics, Nature (London) **612**, 666 (2022).
[16] J. D. Teufel, D. Li, M. S. Allman, K. Cicak, A. J. Sirois, J. D. Whittaker, and R. W. Simmonds, Circuit cavity electromechanics in the strong-coupling regime, Nature (London) **471**, 204 (2011).
[17] E. Verhagen, S. Deléglise, S. Weis, A. Schliesser, and T. J. Kippenberg, Quantum-coherent coupling of a mechanical oscillator to an optical cavity mode, Nature (London) **482**, 63 (2012).
[18] C. Ciuti and I. Carusotto, Input-output theory of cavities in the ultrastrong coupling regime: The case of time-independent cavity parameters, Phys. Rev. A **74**, 033811 (2006).
[19] C. Ciuti, G. Bastard, and I. Carusotto, Quantum vacuum properties of the intersubband cavity polariton field, Phys. Rev. B **72**, 115303 (2005).
[20] S. G. Hofer, W. Wieczorek, M. Aspelmeyer, and K. Hammerer, Quantum entanglement and teleportation in pulsed cavity optomechanics, Phys. Rev. A **84**, 052327 (2011).

[21] P. Forn-Díaz, L. Lamata, E. Rico, J. Kono, and E. Solano, Ultrastrong coupling regimes of light-matter interaction, Rev. Mod. Phys. **91**, 025005 (2019).
[22] A. F. Kockum, A. Miranowicz, S. D. Liberato, S. Savasta, and F. Nori, Ultrastrong coupling between light and matter, Nat. Rev. Phys. **1**, 19 (2019).
[23] S. G. Hofer and K. Hammerer, Entanglement-enhanced time-continuous quantum control in optomechanics, Phys. Rev. A **91**, 033822 (2015).
[24] T. Carmon, M. C. Cross, and K. J. Vahala, Chaotic Quivering of Micron-Scaled On-Chip Resonators Excited by Centrifugal Optical Pressure, Phys. Rev. Lett. **98**, 167203 (2007).
[25] F. M. Buters, H. J. Eerkens, K. Heeck, M. J. Weaver, B. Pepper, S. de Man, and D. Bouwmeester, Experimental exploration of the optomechanical attractor diagram and its dynamics, Phys. Rev. A **92**, 013811 (2015).
[26] F. Monifi, J. Zhang, a. K. Özdemir, B. Peng, Y.-x. Liu, F. Bo, F. Nori, and L. Yang, Optomechanically induced stochastic resonance and chaos transfer between optical fields, Nat. Photonics **10**, 399 (2016).
[27] D. Navarro-Urrios, N. E. Capuj, M. F. Colombano, P. D. García, M. Sledzinska, F. Alzina, A. Griol, A. Martínez, and C. M. Sotomayor-Torres, Nonlinear dynamics and chaos in an optomechanical beam, Nat. Commun. **8**, 14965 (2017).
[28] R. Leijssen, G. R. La Gala, L. Freisem, J. T. Muhonen, and E. Verhagen, Nonlinear cavity optomechanics with nanomechanical thermal fluctuations, Nat. Commun. **8**, ncomms16024 (2017).
[29] J. Shin, Y. Ryu, M.-A. Miri, S.-B. Shim, H. Choi, A. Alù, J. Suh, and J. Cha, On-chip microwave frequency combs in a superconducting nanoelectromechanical device, Nano Lett. **22**, 5459 (2022).
[30] F. Marquardt, J. G. E. Harris, and S. M. Girvin, Dynamical Multistability Induced by Radiation Pressure in High-Finesse Micromechanical Optical Cavities, Phys. Rev. Lett. **96**, 103901 (2006).
[31] N. Lörch, J. Qian, A. Clerk, F. Marquardt, and K. Hammerer, Laser Theory for Optomechanics: Limit Cycles in the Quantum Regime, Phys. Rev. X **4**, 011015 (2014).
[32] L. Bakemeier, A. Alvermann, and H. Fehske, Route to Chaos in Optomechanics, Phys. Rev. Lett. **114**, 013601 (2015).
[33] C. Schulz, A. Alvermann, L. Bakemeier, and H. Fehske, Optomechanical multistability in the quantum regime, Europhys. Lett. **113**, 64002 (2016).
[34] P. Djorwe, Y. Pennec, and B. Djafari-Rouhani, Frequency locking and controllable chaos through exceptional points in optomechanics, Phys. Rev. E **98**, 032201 (2018).
[35] T. J. Kippenberg, H. Rokhsari, T. Carmon, A. Scherer, and K. J. Vahala, Analysis of Radiation-Pressure Induced Mechanical Oscillation of an Optical Microcavity, Phys. Rev. Lett. **95**, 033901 (2005).
[36] M.-A. Miri, G. D'Aguanno, and A. Alù, Optomechanical frequency combs, New J. Phys. **20**, 043013 (2018).
[37] T. F. Roque, F. Marquardt, and O. M. Yevtushenko, Nonlinear dynamics of weakly dissipative optomechanical systems, New J. Phys. **22**, 013049 (2020).
[38] M. Yuan, V. Singh, Y. M. Blanter, and G. A. Steele, Large cooperativity and microkelvin cooling with a three-dimensional optomechanical cavity, Nat. Commun. **6**, 8491 (2015).
[39] A. Noguchi, R. Yamazaki, M. Ataka, H. Fujita, Y. Tabuchi, T. Ishikawa, Koji Usami, and Y. Nakamura, Ground state cooling of a quantum electromechanical system with a silicon nitride membrane in a 3D loop-gap cavity, New J. Phys. **18**, 103036 (2016).
[40] B. Gunupudi, S. R. Das, R. Navarathna, S. K. Sahu, S. Majumder, and V. Singh, Optomechanical Platform with a Three-dimensional Waveguide Cavity, Phys. Rev. Appl. **11**, 024067 (2019).
[41] G. A. Peterson, S. Kotler, F. Lecocq, K. Cicak, X. Y. Jin, R. W. Simmonds, J. Aumentado, and J. D. Teufel, Ultrastrong Parametric Coupling between a Superconducting Cavity and a Mechanical Resonator, Phys. Rev. Lett. **123**, 247701 (2019).
[42] E. E. Wollman, C. U. Lei, A. J. Weinstein, J. Suh, A. Kronwald, F. Marquardt, A. A. Clerk, and K. C. Schwab, Quantum squeezing of motion in a mechanical resonator, Science **349**, 952 (2015).
[43] A. P. Reed, K. H. Mayer, J. D. Teufel, L. D. Burkhart, W. Pfaff, M. Reagor, L. Sletten, X. Ma, R. J. Schoelkopf, E. Knill, and K. W. Lehnert, Faithful conversion of propagating quantum information to mechanical motion, Nat. Phys. **13**, 1163 (2017).
[44] S. Weis, R. Rivière, S. Deléglise, E. Gavartin, O. Arcizet, A. Schliesser, and T. J. Kippenberg, Optomechanically induced transparency, Science **330**, 1520 (2010).
[45] See Supplemental Material at http://link.aps.org/supplemental/10.1103/PhysRevLett.131.067001 for additional experimental results and the theoretical calculations. It includes two additional references, Refs. [46,47].
[46] S. E. Nigg, H. Paik, B. Vlastakis, G. Kirchmair, S. Shankar, L. Frunzio, M. H. Devoret, R. J. Schoelkopf, and S. M. Girvin, Black-Box Superconducting Circuit Quantization, Phys. Rev. Lett. **108**, 240502 (2012).
[47] D. I. Schuster, A. Wallraff, A. Blais, L. Frunzio, R.-S. Huang, J. Majer, S. M. Girvin, and R. J. Schoelkopf, ac Stark Shift and Dephasing of a Superconducting Qubit Strongly Coupled to a Cavity Field, Phys. Rev. Lett. **94**, 123602 (2005).
[48] I. S. Gradshteyn and I. M. Ryzhik, *Table of Integrals, Series, and Products*, 7th ed. (Academic Press, Amsterdam, 2007).
[49] M. A. Lemonde, N. Didier, and A. A. Clerk, Nonlinear Interaction Effects in a Strongly Driven Optomechanical Cavity, Phys. Rev. Lett. **111**, 053602 (2013).
[50] B. D. Hauer, J. Combes, and J. D. Teufel, Nonlinear Sideband Cooling to a Cat State of Motion, Phys. Rev. Lett. **130**, 213604 (2023).
[51] M. I. Dykman, G. Rastelli, M. L. Roukes, and E. M. Weig, Resonantly Induced Friction and Frequency Combs in Driven Nanomechanical Systems, Phys. Rev. Lett. **122**, 254301 (2019).
[52] M. R. Vanner, I. Pikovski, G. D. Cole, M. S. Kim, Č. Brukner, K. Hammerer, G. J. Milburn, and M. Aspelmeyer, Pulsed quantum optomechanics, Proc. Natl. Acad. Sci. U.S.A. **108**, 16182 (2011).